Measurement of Electro-Optic Shock and Electron Acceleration in a Strongly Cavitated Laser Wakefield Accelerator

M. H. Helle,* D. Kaganovich, D. F. Gordon,† and A. Ting
Plasma Physics Division, Naval Research Laboratory, Washington, D.C. 20375, USA
(Received 19 January 2010; published 30 August 2010)

Conically emitted second harmonic radiation was observed when a relativistically intense, ultrashort laser pulse was focused into a jet of gas. This second harmonic electro-optic shock is the result of frequency mixing within the sheath of electrons surrounding a highly cavitated plasma region created by the ponderomotive force of the laser. Strong correlation between the second harmonic characteristics and electron acceleration has been observed.

DOI: 10.1103/PhysRevLett.105.105001 PACS numbers: 52.35.Mw, 41.60.Bq, 42.65.Ky, 52.38.Kd

In the last several years the experimental and theoretical research in the field of plasma-based laser wakefield accelerators has shifted into the blowout regime, or bubble regime, of laser-plasma interaction. In this regime, ambient plasma electrons are fully expelled from the interaction region by the ponderomotive force of a laser pulse that is either self-modulated [1] or shorter than half a plasma period [2], producing a positive core of background ions surrounded by a thin sheath of high density electrons. Theoretical studies predict that under the right conditions the strong electric field inside the bubble can trap and accelerate plasma electrons and eventually produce quasimonoenergetic high energy electron beams [3–5]. Numerous experimental groups [6–8] have demonstrated production of quasimonoenergetic electrons; however, not until very recently has there been any experimental attempt to observe bubble formation [9,10]. One unsolved issue for blowout acceleration is the mechanism by which the plasma background electrons are injected into the bubble field. Kalmykov *et al.* [5] suggested that robust electron trapping can be achieved when the bubble's size is adiabatically evolving. However the focus of that work was on a bubble driven by a laser pulse shorter than half a plasma period. Therefore the mechanism leading to electron injection for self-modulated laser wakefield accelerators operating in the bubble regime still needs to be addressed.

Recent theoretical work by our group suggested that the interaction of the intense laser field with the high density sheath of the plasma bubble drives nonlinear second harmonic source currents that satisfy the conditions required for the formation of an electro-optic shock [11]. These conditions are that the source currents must be contained to a transverse region smaller than the emitted wavelength and exhibit a real Cherenkov angle:

$$\theta_C = \cos^{-1}\frac{v_\phi(2\omega_0)}{v_\phi(\omega_0)} = \cos^{-1}\sqrt{\frac{1-\omega_p^2/\omega_0^2}{1-\omega_p^2/(2\omega_0)^2}}, \quad (1)$$

where v_ϕ is the phase velocity, ω_0 is the laser frequency, and ω_p is the plasma frequency. It is these characteristics that distinguish second harmonic electro-optic shock from other second harmonic mechanisms in plasmas such as nonlinear Thomson scattering. It is the goal of this work to utilize electro-optic shocks as a diagnostic tool for laser wakefield accelerators operating in the bubble regime much in the same way that the Raman instability was used in well behaved wakefields.

We report here that conically emitted second harmonic radiation has been observed in recent self-modulated laser wakefield experiments at the Naval Research Laboratory. We have also observed that there is a strong correlation between the characteristics of the second harmonic and the generation of accelerated electrons, both on axis and off axis [12]. Details of these experimental studies follow.

The experimental setup is shown in Fig. 1. A 10 TW, 50 fs Ti:Sapphire laser system with a central wavelength of 800 nm was focused by a $f/10$ off axis parabola down to a 23 μm diameter vacuum spot producing an intensity of 2.5×10^{18} W/cm^{-2} within a 1 mm long region of He gas. The laser pulse ionized the gas and drove the nonlinear wakefield, while a small, frequency doubled portion of the same pulse probed the region to obtain the plasma density using a folded wave interferometer [13]. The forward scattered radiation of the main pulse was partially reflected

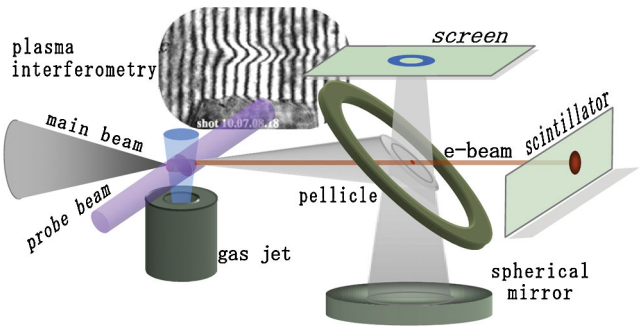

FIG. 1 (color). A schematic of the experimental setup. A collimator and electromagnet (not shown) were placed between the pellicle and scintillator. The top side of the screen was monitored by a CCD camera and an imaging spectrometer (not shown). The scintillator was monitored by an ICCD camera (not shown).

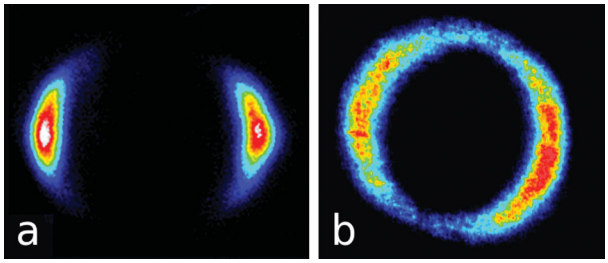

FIG. 2 (color). False color images of the screen seen through a 400 ± 10 nm interference filter for (a) linearly and (b) circularly polarized light generated at a plasma density of 2×10^{19} cm^{-3}. In (a), the laser polarization is horizontal.

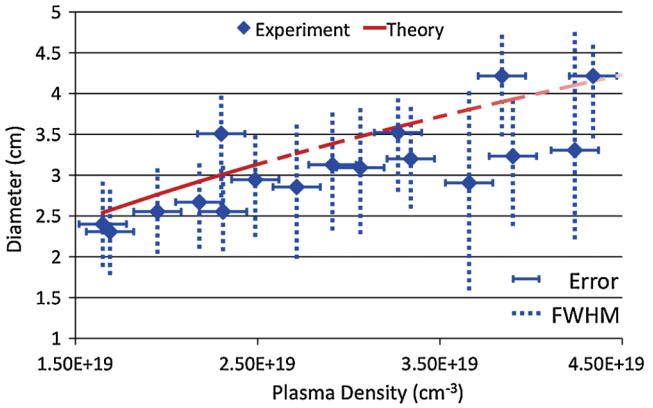

FIG. 3 (color). A plot of the ring diameter versus plasma density. Values extracted from experimental images are plotted and compared to the Cherenkov condition predicted in Ref. [11]. The theory curve becomes dashed above 2.5×10^{19} cm^{-3} to signify the formation of multiple rings. The error associated with the plasma density and the FWHM of the emission have also been included.

by a custom-made pellicle, which helps to eliminate thin film interference. A spherical mirror placed 30 cm from the gas jet, reflected the radiation and back-illuminated a screen placed at the focal plane of the mirror ($f = 15$ cm). This optical system (2D angularly resolved imager) maps the conical emission of the plasma radiation to a 2D polar distribution, where the emission angle θ becomes the radial coordinate [13]. The screen was then monitored by a high resolution CCD camera and imaging prism spectrometer [14]. The slit of the imaging spectrometer was aligned parallel to the linear polarization axis of the laser. In a single shot measurement the imaging spectrometer acquired data over a spectral range of 365 nm to 1100 nm. Additionally, the on axis injected electrons' charge and energy were measured by an electron spectrometer, consisting of collimator, electromagnet, scintillator, and ICCD camera. Off axis electron acceleration was monitored using a scintillator and another ICCD camera.

Single shot data were taken simultaneously using all four diagnostics: plasma interferometry, 2D angularly resolved imaging of the forward radiation, 1D spectral imaging of the forward radiation, and electron spectroscopy. Experimentally we varied two major parameters: plasma density and laser polarization (linear and circular). Plasma density was extracted from the interference pattern using a cylindrically symmetric inverse-Abel transform [15].

To aid in the observation of a second harmonic electro-optic shock produced from a plasma bubble, the experimental parameters were optimized for the generation of high energy, quasimonoenergetic electrons accelerated along the laser axis since these on axis electrons are thought to be a direct consequence of bubble creation [1–5]. On axis quasimonoenergetic electrons ($\sim$40 MeV with $\sim$15% spread) were observed at a plasma density of approximately 4×10^{19} cm^{-3}, see Fig. 6(c). Above and below this plasma density a broad Maxwellian tail of on axis electron energy was observed. No on axis accelerated electrons were observed below a plasma density of 3×10^{19} cm^{-3}. However, at plasma densities between 1.5×10^{19} cm^{-3} and 2×10^{19} cm^{-3} beams of off axis electrons were generated [12].

A second harmonic ring, emitted at the Cherenkov angle, was initially observed at a plasma density of $\sim 1.5 \times 10^{19}$ cm^{-3}. False color images of the screen viewed through a 400 ± 10 nm interference filter are shown in Fig. 2 for (a) linearly and (b) circularly polarized light. The patterns in Fig. 2 are consistent with that expected for an electro-optic shock emitted from the sheath surrounding a plasma bubble. Namely, for linear polarization, the intensity is at a maximum where the electric field is transverse to the electron sheath and at a minimum where it is parallel. For circularly polarized light the intensity evens out since the field is transverse to the entire sheath averaged over an optical cycle [16].

After detecting second harmonic generation, we began probing its characteristics as a function of plasma density to further verify its connection to Cherenkov emission. As the plasma density increased so did the diameter of the ring (emission angle). This is due to the ratio in Eq. (1) decreasing as plasma density increases. Above a plasma density of 2.5×10^{19} cm^{-3}, the second harmonic begins to form multiple rings leading to a spreading of the angular emission envelope. The results of this scan of diameter as a function of plasma density, as well as the corresponding theoretical curve, are shown in Fig. 3. The point where multiple rings began to form is emphasized by turning the theoretical curve into a dashed line. The theoretical curve fits well within the FWHM of the experimental data; however, it appears that the experimental data are shifted slightly to the right when compared to the theoretical curve. We believe this shift is due to an overestimate of the plasma density at each point caused by using the peak of the plasma density profile.

While performing the above mentioned scan of plasma density, spectral data were also taken. The spectral evolution is shown in Fig. 4 for circularly polarized light at three different plasma densities with corresponding false color screen images inserted [17]. In (a), at a plasma density of 2×10^{19} cm^{-3} a single ring, well defined spatially and in

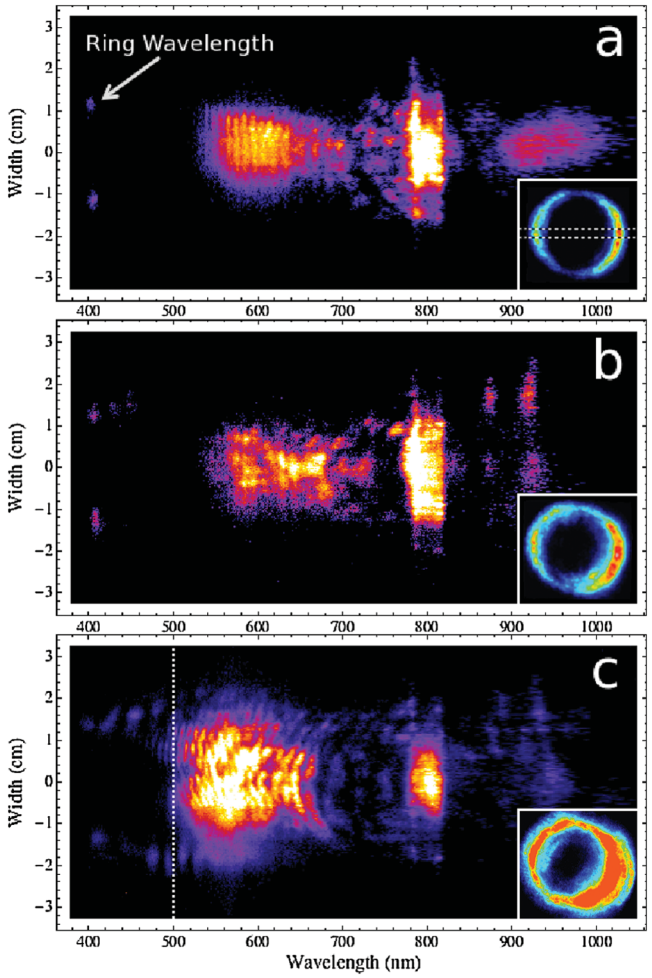

FIG. 4 (color). Imaging spectra extracted from the imaging spectrometer with corresponding false color images (amplitude not to scale). The dashed region shown in the insert of figure (a) indicates where the spectrum was extracted. Spectra are shown for plasma densities of (a) 2×10^{19} cm^{-3}, (b) 2.5×10^{19} cm^{-3}, and (c) 3×10^{19} cm^{-3}. The region left of the dashed line in (c) is reproduced in Fig. 5(a) for comparison to theory. A diffraction-like pattern around 600 nm is a consequence of the pellicle response and intensity comparisons are not meaningful across large wavelength ranges.

wavelength, was observed. When a density of 2.5×10^{19} cm^{-3} was reached (b), multiple rings of increasing size and wavelength began to appear. At an even higher density of 3×10^{19} cm^{-3} (c), the image on the screen started to appear chaotic and these multiple rings became fully formed. Because of the narrow spectral range of the 400 nm filter and spectral overlap, it is difficult to see the multiple rings in the screen images, but they are more apparent in the imaging spectra.

These multiple rings are reproduced in Fig. 5(a) for added emphasis and can be explained as a consequence of multiple bubble formation. Qualitatively, multiple bubbles will individually emit second harmonic radiation producing a train of pulses spaced according to the bubble spacing. The spectrum of such a temporal structure will

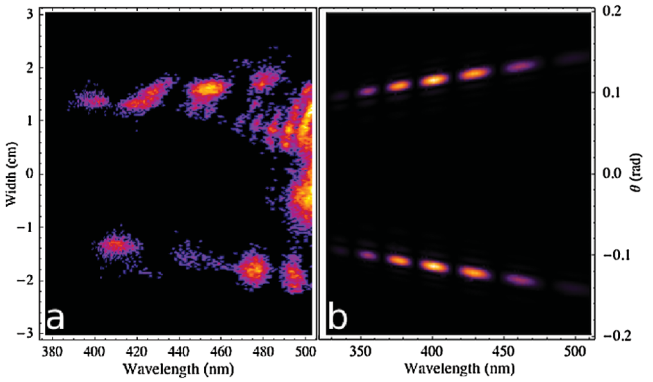

FIG. 5 (color). An enlarged false color image of the 380 nm to 500 nm range of Fig. 4(c) is shown in (a) as a comparison to (b), the theoretical prediction for the spectrum of an electro-optic shock using two bubbles. The theoretical prediction extends into the UV which is beyond the spectrometer's cutoff of 365 nm.

itself be modulated as observed in Fig. 5(a). This spectrum can be reproduced analytically, as shown in Fig. 5(b), from Eq. (2) of Ref. [11]. Using the notation described in Ref. [11], where $g(z)$ is the axial variation of the sheath density at $t = 0$, $h(z)$ is the variation of the sheath density with propagation distance, and v is the velocity of the bubble which is assumed to be constant, the spectral intensity in the far field, as a function of the polar angle θ, can be expressed as

$$|A(\omega, \theta)|^2 = A_0^2 |\hat{g}(-\delta\omega/v)\hat{h}(K) J_1(k\rho_0 \sin\theta)|^2.$$

Here, $k^2c^2 = \omega^2 - \omega_p^2$, $\delta\omega = \omega - 2\omega_0$, $K = 2k_0 + \delta\omega/v - k\cos\theta$ which gives the Cherenkov condition, ω_p is the ambient plasma frequency, ω_0 is the laser frequency, and A_0 is a factor independent of ω and θ. The circumflex denotes Fourier transformation.

If the propagation distance is short, the effect of $\hat{h}$ is to force the emission into a poorly defined cone angle for each frequency component. With the Bessel function dependence being weak, the frequency spectrum is then determined mostly by $\hat{g}$, where $\hat{g}$ is just the axial Fourier transform of the sheath density. Therefore the observed modulated spectrum has to be due to a modulated sheath density. The fact that there are several modulation periods indicates that the peaks are narrow relative to their separation. Furthermore, the wide angular spread observed in Fig. 5(a) suggests that the bubble propagation distance was relatively short. Iterating the parameters with these constraints in mind leads to Fig. 5(b). The parameters used to generate Fig. 5(b) correspond to a pair of cylindrical sheaths (two bubbles) separated by 6 μm ($\sim\lambda_p$ for a 3×10^{19} cm^{-3} plasma), with equal densities, and individual lengths of 2 μm. A propagation distance of 150 μm was used. The bubble lengths and propagation distance were found based on the observed second harmonic bandwidth and the emission spread, respectively. The resemblance with the second harmonic region of the angular-spectral distribution from Fig. 5(a) is remarkable. Electro-optic

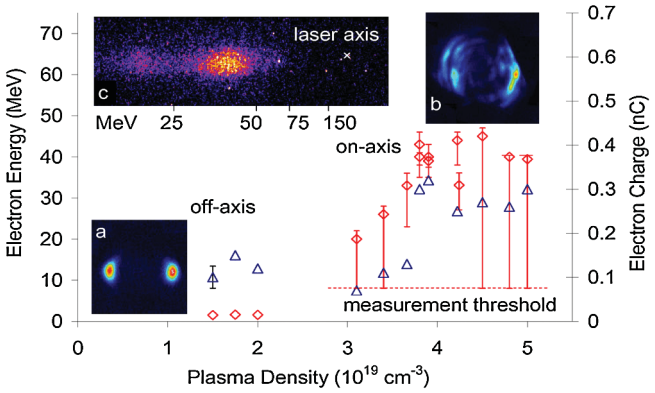

FIG. 6 (color). A plot of energy peak (◇) and total charge (△) versus plasma density for off axis and on axis electron generation. Bars extending from the energy measurements signify the energy spread. Note the narrow energy spread at a plasma density of 4×10^{19} cm^{-3}. For clarity, error bars for charge measurements are shown on one data point. Inserted are typical second harmonic false color images observed (a) when off axis electrons are generated and (b) when on axis electrons are generated. Additionally, an electron spectrum of quasimonoenergetic electrons recorded at a plasma density of 4.25×10^{19} is inserted in (c).

shock produced by the sheaths of two or more distinct bubbles is expected when the plasma density is raised since raising it corresponds to increasing the number of plasma periods within the laser pulse.

The correlation between this radiation and electron beam production can be seen in Fig. 6 as a plot of electron energy peak and total charge measured versus plasma density for both off axis and on axis accelerated electrons using linearly polarized light. Inserted are false color images of the second harmonic ring corresponding to (a) off axis and (b) on axis electron generation. It was observed that the second harmonic was first generated at the same narrow range of plasma densities that off axis electrons were detected. Electron energy for off axis electrons were presented earlier by Kaganovich *et al.* [12]. Accelerated electrons were produced on axis starting at a plasma density of 3×10^{19} cm^{-3}, concurrent with the appearance of multiple rings, i.e., multiple bubble formation.

In Fig. 6, the on axis electrons were first observed with a large Maxwellian energy spread extending to zero. Approaching 4×10^{19} cm^{-3}, the energy spread begins to diminish and a quasimonoenergetic beam with an energy of ~40 MeV appeared. A representative electron spectrum is shown in insert (c), which also exhibits a secondary beam much like that attributed to multiple bubbles in Ref. [1]. As the plasma density was increased further the quasimonoenergetic feature disappeared and the electron energy spectrum became a broad Maxwellian tail again.

Based on these observations there appears to be a strong correlation between bubble generation and electron acceleration for a self-modulated laser wakefield. It is our conjecture that once a bubble is formed, accelerated yet untrapped plasma electrons at the trailing edge of the bubble appear as an off axis electron beam [12]. We believe self-injection occurs when the trailing edge of a bubble is dynamically modified by the formation of multiple bubbles within the laser envelope. These injected and trapped electrons are then accelerated to high energy within the wakefield. A beam with small energy spread can be produced when the beam is accelerated through a distance matching the dephasing length, $L_d \approx 150$ μm for these high plasma densities [1,18].

In conclusion we have indirectly detected the existence of a thin sheath of electrons that characterize plasma bubbles generated in the blowout regime of self-modulated laser wakefield accelerators. Using this diagnostic, a correlation between bubble formation and electron trapping and acceleration has been established. There is experimental evidence that background plasma electrons are trapped into the acceleration structure when multiple bubbles are created due to the self-modulation of the laser beam in the plasma. These electrons are then further accelerated forming a quasimonoenergetic beam at the dephasing length.

This work was supported by the Office of Naval Research and the Department of Energy. We acknowledge discussions with B. Hafizi and E. Van Keuren.

*Department of Physics, Georgetown University, Washington, D.C. 20057, USA.
†Corresponding author: daniel.gordon@nrl.navy.mil

[1] B. Hidding *et al.*, Phys. Plasmas **16**, 043105 (2009).
[2] W. Lu *et al.*, Phys. Rev. ST Accel. Beams **10**, 061301 (2007).
[3] I. Kostyukov, A. Pukhov, and S. Kiselev, Phys. Plasmas **11**, 5256 (2004).
[4] W. Lu *et al.*, Phys. Rev. Lett. **96**, 165002 (2006).
[5] S. Kalmykov *et al.*, Phys. Rev. Lett. **103**, 135004 (2009).
[6] S. Mangles *et al.*, Nature (London) **431**, 535 (2004).
[7] J. Faure *et al.*, Nature (London) **444**, 737 (2006).
[8] W. P. Leemans *et al.*, Nature Phys. **2**, 696 (2006).
[9] P. Dong *et al.*, Phys. Rev. Lett. **104**, 134801 (2010).
[10] J. E. Ralph *et al.*, Phys. Rev. Lett. **102**, 175003 (2009).
[11] D. F. Gordon *et al.*, Phys. Rev. Lett. **101**, 045004 (2008).
[12] D. Kaganovich, D. F. Gordon, and A. Ting, Phys. Rev. Lett. **100**, 215002 (2008).
[13] E. Hecht, *Optics* (Addison-Wesley, Reading, Mass., 2002), 4th ed., ISBN 0805385665.
[14] J. M. Lerner, Cytometry Part A **69A**, 712 (2006).
[15] M. Takeda, H. Ina, and S. Kobayashi, J. Opt. Soc. Am. **72**, 156 (1982).
[16] D. F. Gordon, B. Hafizi, and A. Ting, Opt. Lett. **34**, 3280 (2009).
[17] Wide Raman bands on both the Stokes and anti-Stokes sides of the fundamental were clearly present. These sidebands provide insight into the modulation of the laser pulse by the plasma and are the subject of future work.
[18] C. T. Hsieh *et al.*, Phys. Rev. Lett. **96**, 095001 (2006).